scientific reports

Check for updates

OPEN

Synthesis and antitumor evaluation of amino acid conjugates of monocarbonyl curcumin in hepatocellular carcinoma cell

Weiya Cao[1,2], Pan Yu[1,3]✉, Yongchang Cao[1], Shuhui Feng[1] & Nan Yin[1]

Curcumin possesses a variety of pharmacological properties, particularly anticancer activity. However, its clinical utility is limited by its poor water solubility and low bioavailability. To alleviate the problems, our previous research demonstrated that mono-carbonyl curcumin easters can be employed for the development of novel anticancer agents. In this study, further structural optimization was performed and a series of novel amino acid conjugates of mono-carbonyl curcumin H1-H6 were designed, synthesized, and evaluated by in vitro and in vivo studies. Compound H1 was found as the most potent derivative (IC_{50} = 8.66 μM) compared to curcumin (IC_{50} = 36.19 μM) by anti-proliferation assay. Subsequently, wound healing, transwell, JC-1 staining, the HepG2 cell xenograft model and H&E staining experiments were performed, and it was found that compound H1 was more effective than curcumin in inhibiting tumor growth. The results of transcriptome sequence, bioinformatics analysis, molecular docking, and western blotting suggested that compound H1 could inhibit cell proliferation and induce apoptosis through the AKT/FOXO1 pathway. Hence, H1 is a promising lead compound with the potential to be developed as a chemotherapy agent for hepatocellular carcinoma.

Keywords Mono-carbonyl Curcumin, Amino acid conjugates, Anti-hepatoma activity, AKT/FOXO1 pathway, Molecular Docking, Xenograft model

Curcumin is a hydrophobic polyphenol from the rhizome of the plant *Curcuma longa*with a broad spectrum of pharmacological activities, especially antitumor activity[1–4]. However, clinical investigations using curcumin did not show great benefit due to its poor bioavailability[5,6]. A series of modifications have been performed on the β-diketone structure and hydroxy on benzene of curcumin, which could largely enhance stability, bioavailability, and antitumor activity[7–10].

Our previous research showed that mono-carbonyl curcumin cinnamyl ester **B5** and phenylmethyl ester **G2**greatly increased anti-human hepatocellular carcinoma (HCC) activity, which converted the diketone structure into a single ketone and modified hydroxy on benzene of curcumin with natural organic acids[11,12]. The results of molecular dynamics simulations and pharmacological experiments suggested the subsequent structural optimization may focus on shortening the carbon chain modification on hydroxy on benzene suitably and introducing a moiety with better water solubility. The mechanism of curcumin and its derivatives was also simply explored in our previous research and may relate to the influence of the HepG2 cell metabolic process through inhibition of the expression of AKT protein. However, how AKT regulates downstream signaling molecules remains unclear and it is important to investigate urgently the mechanism for anticancer effects of Traditional Chinese Medicine.

Amino acids are the primary construction blocks for proteins with biological activities and a broader shift can result in structural modification accounting for amino acids containing a variety of sidechains[13–15]. Among the amino acid and natural compound conjugates, oncolytic peptides-anticancer compounds based conjugates represent promising novel candidates for anticancer treatments[16–18]. To date, several amino acid and natural compound conjugates have been reported that involve curcumin, astaxanthin and quercetin to enhance the pharmacological activities, which may be attributed to their better solubility, enhanced accumulation in the cells, resulting from better cellular uptake and decreased metabolic rate[19–21]. These ester linkages are biodegradable by

[1]College of Public Health, Anhui University of Science and Technology, Hefei 230000, China. [2]Joint Research Center of Occupational Medicine and Health, Institute of Grand Health, Hefei Comprehensive National Science Center, Hefei 230000, China. [3]The First Affiliated Hospital of Anhui University of Science and Technology (Huainan First People'S Hospital), Huainan 232001, China. ✉email: 2020035@aust.edu.cn

esterase enzymes and therefore these conjugates may be acting as prodrugs[22,23]. Moreover, the assessment of their antiproliferative activities suggested that diesters of curcumin were relatively more active than curcumin itself and the monoester of curcumin in HeLa and KB cancer cells due to their increased solubility, slow metabolism and better cellular uptake[24]. Therefore, it is a strategy that introduces natural products such as amino acids on the hydroxy of mono-carbonyl curcumin to increase the anti-HCC activity.

In this study, six highly water-soluble amino acid conjugates **H1**-**H6** of mono-carbonyl curcumin were synthesized through structural modification of curcumin. The anti-HCC activities of the conjugates were assessed by a series of in vitro and in vivo experiments including MTT assay, clone formation, wound healing, transwell migration, JC-1, Xenograft model, H&E staining analysis, molecular docking, western blot and some informatics analysis. The study findings will establish a groundwork for the application of optimizing curcumin in the field of anticancer drugs.

Materials and methods

Chemistry

General

All solvents and reagents were analytical grade and purchased from Shanghai Titan Technology Co., LTD. ^{1}H NMR and ^{13}C NMR spectra for the compounds were recorded with Bruker AM 600 MHz and 400 MHz spectrometers using $CDCl_3$ solvent. Coupling constants (J values) are given in Hz. Melting points (M.P.) were determined on an SRS OptiMelt-100 instrument and ESI-MS was recorded on an Agilent 6520B Q-TOF system. Reactions were monitored by thin-layer chromatography (TLC) on a glass plate coated with silica gel with the fluorescent indicator (GF254). Column chromatography (CC) was performed on silica gel (200–300 mesh; Qingdao Makall Group Co., Ltd.; Qingdao, China).

Preparation of mono-carbonyl Curcumin derivatives H1–H6

The starting material mono-carbonyl curcumin **1** (Fig. 1) was synthesized from 4-hydroxy-3-methoxybenzaldehyde by the same procedure as described in our previous article[11]. Specifically, the review emphasizes the role of D-amino acids and D-type amino acids-based conjugates in evading proteolytic cleavage and enhancing tumor accumulation through stereochemical-driven interactions, and the principles directly informed our design of curcumin-D-alanine conjugates[25]. Six amino acids (glycine, D-alanine, L-valine, L-leucine, L-methionine, L-phenylalanin) were protected by introducing Boc group to the amino group with Et_3N and $(Boc)_2O$ in water and acetone mixture solvents at 0–40 ℃ for 4 h. Boc-amino acids (**2a**-**2f**), mono-carbonyl curcumin **1**, 1-(3-dimethylaminopropyl)−3-ethylcarbodiimide (EDCI), 4-dimethylaminopyridine (DMAP) were combined with dichloromethane and allowed to react at 25 ℃ for 7–12 h under inert gas to obtain Boc-amino acids curcumin (**3a**-**3f**). Subsequently, compounds **3a**-**3f** were allowed to react with 2 mol/L hydrochloric acid in methanol solution at 0 ℃ for 2–3 h to deprotect the Boc group and produce amino acid conjugates of mono-carbonyl curcumin **H1**-**H6**.

Biological assays

Cell culture

Human hepatocellular carcinoma cell line HepG2 was obtained from Nanjing Forestry University. MTT (3-(4,5-Dimethylthiazol-2-yl)−2,5-diphenyltetrazolium bromide) was purchased from Sigma. 6-well, 24-well and 96-well plates were purchased from Beyotime Biotechnology. Cells were grown in DMEM medium with 10% fetal bovine serum at 37 °C and 5% CO_2. All compounds were dissolved in DMSO and the final concentration had no effects on cell viability.

MTT assay

Seed HepG2 cells (5000 cells/well) in a 96-well plate and allow them to adhere. The wells were treated with mono-carbonyl curcumin derivatives **H1**-**H6**with different concentrations and incubated for 48 h. Then, 20 μL, 4 mg/mL MTT of PBS solution was added to each well, allowing viable cells to reduce MTT to formazan crystals.

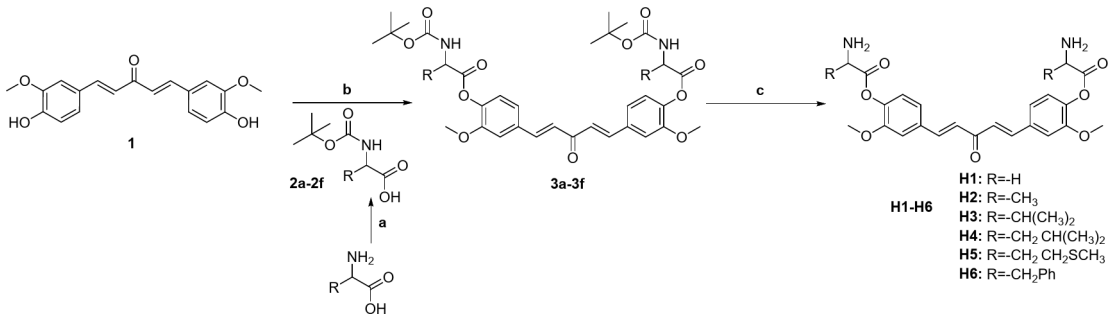

Fig. 1. Synthesis of amino acid conjugates of mono-carbonyl curcumin **H1**-**H6**. Reagents and conditions: (a) $(BOC)_2O$, triethylamine, acetone and water, 0–40 ℃, 4 h; (b) EDCI, DMAP, N_2 protection, CH_2Cl_2, 7–12 h; (c) 2 M HCl in CH_3OH solution, 0℃, 2–3 h.

Add 200 µL of DMSO to dissolve the formazan crystals and measure absorbance at 490 nm to determine cell viability on a Super Microplate Reader (MQX2OO) (BioTek, the United States)[26].

Clone formation assay
HepG2 cell line (500 cells per well) was seeded into each well of a 6-well plate. The colonies were formed at 37 °C in a CO_2 incubator for 14 days. Subsequently, the colonies were fixed with 4% paraformaldehyde and stained with 0.1% crystal violet solution for visualization[27].

Wound healing assay
A monolayer of HepG2 cells (1.5×10^5cells/ well) was put into 24-well plates and allowed to grow until it reached 80–90% confluence. Use a sterile pipette tip to create a straight line (wound) across the cell monolayer. The detached cells were rinsed gently with PBS. The cells were subjected to the target compound at different concentrations in fresh DMEM medium and subsequently cultured for 24–48 h. The cell migration was quantified and the percentage of wound closure over time was calculated by measuring the wound width using a DMIL LED 3000 inverted microscope (Leica, Wetzlar, Germany)[28].

Transwell migration assay
The upper and lower chambers were separated by placing transwell inserts in a 24-well plate. HepG2 cells (5×10^4cells/ well) were incubated in the upper chamber of each insert and the target compound was added to the lower chamber to promote cell migration through the pores. After incubation for 48 h, remove the inserts and fix the cells on the upper side of the membrane with 4% paraformaldehyde. Stain the migrated cells using crystal violet and count the stained cells on the lower side of the membrane to quantify migration under a microscope[29].

Mitochondrial membrane potential assay
HepG2 cells were treated with the target compound in a 6-well plate for 48 h to induce changes in mitochondrial function. The medium was removed and washed with PBS. The cells were added to the JC-1 staining solution and incubated for 20 min at 37 °C. After incubation, the cells were washed twice with PBS to remove excess dye. The cells were then analyzed using a fluorescence microscope and measured both green (488 nm) and red (550 nm) fluorescence intensities. Calculate the ratio of red to green fluorescence intensity. A higher red/green ratio indicates a healthy mitochondrial membrane potential, while a lower ratio suggests mitochondrial dysfunction[11].

Xenograft model and in vivo study
All animal experiments were conducted with the approval of the Animal Care and Use Committee of Anhui University of Science and Technology (License No: S22023017) and in compliance with the Guide for the Care and Use of Laboratory Animals by the National Institutes of Health. The study is reported in accordance with ARRIVE guidelines (https://arriveguidelines.org). The BALB/c nude mice (female, 6–8 weeks, about 20 g) were purchased from Nanjing Junke Biological Co., LTD. Animal welfare and experimental procedures were kept according to the Guide for Care and Use of Laboratory Animals (National Institutes of Health, the United States) and the system guidance of the Anhui University of Science and Technology Animal Management Committee. Mice were anesthetized using the isoflurane gas inhalation anesthesia method. Briefly, HepG2 cell suspension (2×10^6 cells in 100 µL) was subcutaneously injected into the right flank of nude mice using a sterile syringe. Monitor the mice post-injection for any signs of distress or complications. Provide analgesics as necessary. Place the mice in a suitable housing environment with proper bedding, food, and water. Body weights and tumor size were measured every 3 days. The tumor volume was calculated using the formula: $0.5 \times L \times (W)^2$, where L and W are the length and width of the tumor mass, respectively. The mice can be euthanized according to ethical guidelines at predetermined time points or when tumors reach a certain size (100 mm^3). The tumors were harvested for further analysis such as H&E staining[30]. At the endpoint, the mice were euthanized post-modeling using pentobarbital sodium.

H&E staining analysis
The tissue slide was deparaffinized by immersion in xylene (2 changes, 10–15 min each), followed by 100% ethanol (2 changes), then 95% and 70% ethanol. After being rinsed in distilled water, stained with hematoxylin (5–10 min), differentiated with 1% HCl and 70% ethanol, immersed in ammonia water, stained with eosin (30 s to 2 min), dehydrated in ethanol and xylene, the slide sample was mounted using a coverslip with mounting medium and dried for a few hours and then observed under a light microscope[31].

GO and KEGG analysis
Enrichment analysis of gene ontology (GO) function and Kyoto encyclopedia of genes and genomes (KEGG) pathway was performed using the online David (https://david.ncifcrf.gov/) database, and $P < 0.05$ was used as the evaluation criterion. The top 10 biological functions including cellular components (CC), molecular functions (MF), and biological processes (BP), and the top 30 signaling pathways in the results were selected for visual analysis. The column and bubble graphs analyzed by GO and KEGG analysis were finally also conducted[32].

Survival analysis and pathological staging
The survival analysis and pathological staging of AKT and FOXO1 were carried out by the platform GEPIA2 (http://gepia2.cancer-pku.cn/)[33]. In the GEPIA2 server, Kaplan-Meier survival curves and box plots of liver

cancer stage were constructed to examine the relationship between the hub genes and the overall survival and pathological staging of liver cancer patients.

Molecular docking studies

The molecular docking technique was performed using the Glide module in Schrodinger 2017 to explore the interaction mode between the test compounds and AKT and FOXO1 proteins[34]. The crystal structure of AKT (PDB ID: 3O96) and FOXO1 (PDB ID: 6AEJ) was downloaded from the Protein Data Bank[35]. The initial structures were prepared with the Protein Preparation Wizard workflow and the receptor grid was generated according to the endogenous ligand. The small molecules were optimized with the LigPrep workflow and minimized using the OPLS-2005 force field with the conformational search method. All other parameters were set as default and the binding affinity was evaluated by the binding free energy (Kcal/mol) with standard precision (SP) docking mode. Finally, plausible docking models were selected from the abundant clusters between the ligand and receptor that had lower binding energies and intermolecular interactions were illustrated using PyMOL software.

Western blot analysis

HepG2 cells in 6-well plates were rinsed twice with cold PBS and lysed on ice for 30 min. After centrifugation, the protein concentrations were measured using the BCATM protein quantification kit (Beyotime Biotechnology). Antibodies against phospho-AKT (D9E), FOXO1 (C29H4), p27 Kip1 (D69C12), phospho-Bcl2 (5H2), cleaved-caspase 3 (5AE1) and β-actin (13E5) were purchased from CST. Briefly, the quantified protein samples were subjected to an SDS-PAGE and then transferred to a PVDF membrane. After incubating with primary antibodies at 4 °C overnight and secondary antibodies at room temperature for 2 h, the membrane was illuminated with ECL solution and the density was analyzed using Image J[36].

Results and discussion

General method for synthesis of Boc-amino acids 2a-2f

Six amino acids (20 mmol) were dissolved with 20 mL water and 40 mL acetone in the flask, Et_3N (1.5 equivalent) and $(Boc)_2O$ (22 mmol) were added under agitation at a controlled temperature of 0–40 ℃ for 4 h. The reaction mixture was monitored using TLC and the acetone was evaporated under reduced pressure. Then the water layer was acidized with dilute HCl to 2–3 (pH value) and was extracted with ethyl acetate (4 × 60 mL). The combined organic layer was then washed with saturated salt (2 × 10 mL), and dried over anhydrous sodium sulfate. The obtained crude product was crystallized with ethyl acetate and petroleum ether (1: 2, volume ratio) and relevant Boc-amino acids **2a-2f** were obtained (90–95% yield).

Boc-Glycine (2a) Yield: 93%. ESI-MS *m*/*z* $(M-H)^-$: calculated 174.08, measured 174.18. M.P.:86–88 °C. ^1H NMR (600 MHz, $CDCl_3$) δ 11.30 (s, 1H), 3.92 (d, *J* = 40.8 Hz, 2 H), 1.41 (s, 9 H). ^{13}C NMR (151 MHz, $CDCl_3$) δ 174.64, 156.22, 81.94, 80.50, 43.42, 42.26, 28.35.

Boc-D-Alanine (2b) Yield: 93%. ESI-MS *m*/*z* $(M-H)^-$: calculated 188.10, measured 188.21. M.P.:81–83 °C. ^1H NMR (600 MHz, $CDCl_3$) δ 7.92 (s, 1H), 4.23 (d, *J* = 112.4 Hz, 1H), 1.42 (s, 9 H), 1.40 (d, *J* = 7.2 Hz, 3 H). ^{13}C NMR (151 MHz, $CDCl_3$) δ 177.58, 155.62, 81.74, 80.37, 50.34, 49.21, 28.40, 18.45.

Boc- L-Valine (2c) Yield: 90%. ESI-MS *m*/*z* $(M-H)^-$: calculated 216.13, measured 216.26. M.P.:77–79 °C. ^1H NMR (600 MHz, $CDCl_3$) δ 11.66 (s, 1H), 4.12 (d, *J* = 138.7 Hz, 1H), 2.33–2.00 (m, 1H), 1.43 (s, 9 H), 0.94 (dd, *J* = 39.8, 6.8 Hz, 6 H). ^{13}C NMR (151 MHz, $CDCl_3$) δ 177.29, 155.99, 81.76, 80.17, 60.21, 58.54, 31.19, 28.42, 19.12, 17.56.

Boc-L-Leucine (2d) Yield: 92%. ESI-MS *m*/*z* $(M-H)^-$: calculated 230.15, measured 230.29. M.P.:85–87 °C. ^1H NMR (600 MHz, $CDCl_3$) δ 6.88 (s, 1H), 4.83 (d, *J* = 164.2 Hz, 1H), 4.21 (d, *J* = 104.1 Hz, 1H), 1.43 (s, 9 H), 0.94 (d, *J* = 6.6 Hz, 6 H). ^{13}C NMR (151 MHz, $CDCl_3$) δ 178.01, 155.86, 81.72, 80.31, 53.33, 52.14, 41.56, 28.43, 24.92, 22.96, 21.90.

Boc-L-methionine (2e) Yield: 95%. ESI-MS *m*/*z* $(M-H)^-$: calculated 248.10, measured 248.33. M.P.:47–49 °C. ^1H NMR (600 MHz, $CDCl_3$) δ 10.29 (s, 1H), 4.51–4.21 (m, 1H), 2.56 (t, *J* = 7.1 Hz, 2 H), 2.22–2.12 (m, 1H), 2.09 (s, 3 H), 2.02–1.92 (m, 1H), 1.43 (s, 9 H). ^{13}C NMR (151 MHz, $CDCl_3$) δ 176.96, 155.74, 82.18, 80.51, 53.63, 52.80, 31.93, 30.07, 28.39, 15.49.

Boc-L-Phenylalanine (2f) Yield: 94%. ESI-MS *m*/*z* $(M-H)^-$: calculated 264.13, measured 264.31. M.P.:85–87 °C. ^1H NMR (600 MHz, $CDCl_3$) δ 11.77 (s, 1H), 7.34–7.27 (m, 3 H), 7.22 (dd, *J* = 15.7, 7.1 Hz, 2 H), 4.54 (d, *J* = 145.3 Hz, 1H), 3.29–2.87 (m, 2 H), 1.38 (d, *J* = 80.2 Hz, 9 H). ^{13}C NMR (151 MHz, $CDCl_3$) δ 176.73, 155.47, 136.63, 135.98, 129.51, 128.67, 127.18, 81.71, 80.38, 56.22, 54.37, 39.32, 37.94, 28.40.

General method for synthesis of mono-carbonyl curcumin Boc-amino acid conjugates 3a-3f

A solution of mono-carbonyl curcumin **1** (1 g, 3.1 mmol) and Boc-amino acids (7.5 mmol) in CH_2Cl_2 (25 ml) was taken in a round-bottomed flask. DMAP (1.5 mmol) was added to the reaction mixture and stirred for 0.5 h. After this EDCI (7.5 mmol) was added and set for stirring until the completion of the reaction (7–12 h) under a nitrogen atmosphere. The progress of the reaction was monitored by TLC analysis. The reaction mixture was then added H_2O and extracted with CH_2Cl_2. The combined organic layer was dried over anhydrous sodium sulfate and was purified by flash chromatography with ethyl acetate/petroleum ether to give these yellow compounds **3a**-**3f**. The yields were between 51.3% and 61.5%.

((1E,4E)−3-oxopenta-1,4-diene-1,5-diyl)bis(2-methoxy-4,1-phenylene) bis(2-((tert-butoxycarbonyl)amino)acetate) (3a) Yield: 60.8%. ESI-MS *m*/*z*: 639.69 (M-H)$^-$. ^{1}H NMR (600 MHz, $CDCl_3$) δ 7.45 (d, *J* = 16.2 Hz, 1H), 7.15–7.05 (m, 3 H), 6.65 (d, *J* = 16.2 Hz, 1H), 4.21 (d, *J* = 5.5 Hz, 1H), 3.83 (s, 3 H), 2.37 (s, 2 H), 1.45 (s, 9 H). ^{13}C NMR (151 MHz, $CDCl_3$) δ 198.35, 168.57, 155.78, 151.39, 142.68, 141.25, 133.77, 127.56, 123.29, 121.59, 111.43, 80.32, 56.02, 42.39, 28.41, 27.63.

((1E,4E)−3-oxopenta-1,4-diene-1,5-diyl)bis(2-methoxy-4,1-phenylene) bis(2-((tert-butoxycarbonyl) amino)propanoate) (3b) Yield: 55.8%. ESI-MS *m*/*z*: 667.74 (M-H)$^-$. ^{1}H NMR (600 MHz, $CDCl_3$) δ 7.47 (d, *J* = 16.2 Hz, 1H), 7.13 (q, *J* = 11.3, 10.4 Hz, 3 H), 6.66 (d, *J* = 16.2 Hz, 1H), 5.09 (s, 1H), 4.60 (s, 1H), 3.85 (s, 3 H), 2.39 (s, 3 H), 1.46 (s, 9 H). ^{13}C NMR (151 MHz, $CDCl_3$) δ 198.33, 183.23, 155.23, 151.47, 142.74, 141.53, 133.74, 127.59, 123.34, 121.68, 111.43, 56.09, 49.46, 29.86, 28.48, 27.70, 18.88.

((1E,4E)−3-oxopenta-1,4-diene-1,5-diyl)bis(2-methoxy-4,1-phenylene) bis(2-((tert-butoxycarbonyl) amino)−3-methylbutanoate) (3c) Yield: 53.4%. ESI-MS *m*/*z*: 723.85 (M-H)$^-$. ^{1}H NMR (600 MHz, $CDCl_3$) δ 7.46 (d, *J* = 16.2 Hz, 1H), 7.14–7.11 (m, 2 H), 7.07 (d, *J* = 8.0 Hz, 1H), 6.66 (d, *J* = 16.2 Hz, 1H), 5.09 (s, 1H), 4.52 (s, 1H), 3.83 (s, 3 H), 1.46 (s, 9 H), 1.09 (d, *J* = 6.8 Hz, 3 H), 1.03 (d, *J* = 6.8 Hz, 3 H). ^{13}C NMR (151 MHz, $CDCl_3$) δ 198.34, 170.47, 155.84, 151.47, 142.74, 141.43, 133.73, 127.55, 123.44, 121.64, 111.38, 80.09, 58.69, 55.86, 31.43, 28.45, 27.66, 19.22, 17.34.

((1E,4E)−3-oxopenta-1,4-diene-1,5-diyl)bis(2-methoxy-4,1-phenylene) bis(2-((tert-butoxycarbonyl) amino)−4-methylpentanoate) (3d) Yield: 51.3%. ESI-MS *m*/*z*: 751.90 (M-H)$^-$. ^{1}H NMR (600 MHz, $CDCl_3$) δ 7.45 (d, *J* = 16.2 Hz, 1H), 7.10 (t, *J* = 13.0 Hz, 3 H), 6.64 (d, *J* = 16.2 Hz, 1H), 4.99 (s, 1H), 4.56 (s, 1H), 3.82 (s, 3 H), 1.83 (d, *J* = 19.9 Hz, 2 H), 1.67–1.60 (m, 1H), 1.45 (s, 9 H), 1.00 (d, *J* = 5.8 Hz, 6 H). ^{13}C NMR (151 MHz, $CDCl_3$) δ 198.29, 171.52, 155.51, 151.46, 142.74, 141.55, 133.61, 127.46, 123.35, 121.61, 111.39, 80.06, 55.96, 52.34, 41.76, 28.41, 27.61, 24.90, 23.02, 21.99.

((1E,4E)−3-oxopenta-1,4-diene-1,5-diyl)bis(2-methoxy-4,1-phenylene) bis(2-((tert-butoxycarbonyl) amino)−4-(methylthio)butanoate) (3e) Yield: 61.5%. ESI-MS *m*/*z*: 787.97 (M-H)$^-$. ^{1}H NMR (600 MHz, $CDCl_3$) δ 7.46–7.42 (m, 1H), 7.12–7.02 (m, 3 H), 6.64 (d, *J* = 16.2 Hz, 1H), 5.28 (s, 1H), 4.69 (s, 1H), 3.82 (s, 3 H), 2.34 (d, *J* = 13.5 Hz, 4 H), 2.12 (s, 3 H), 1.44 (s, 9 H). ^{13}C NMR (151 MHz, $CDCl_3$) δ 198.26, 170.43, 151.26, 142.60, 141.25, 133.74, 127.52, 124.96, 123.54, 121.57, 114.98, 111.33, 109.51, 80.24, 55.91, 53.01, 29.87, 28.36, 27.59, 15.51.

((1E,4E)−3-oxopenta-1,4-diene-1,5-diyl)bis(2-methoxy-4,1-phenylene) bis(2-((tert-butoxycarbonyl) amino)−3-phenylpropanoate) (3f) Yield: 58.2%. ESI-MS *m*/*z*: 819.94 (M-H)$^-$. ^{1}H NMR (600 MHz, $CDCl_3$) δ 7.46 (d, *J* = 16.2 Hz, 1H), 7.37–7.31 (m, 2 H), 7.28 (d, *J* = 7.1 Hz, 3 H), 7.13 (d, *J* = 6.5 Hz, 2 H), 7.01 (d, *J* = 8.3 Hz, 1H), 6.66 (d, *J* = 16.2 Hz, 1H), 5.02 (d, *J* = 8.1 Hz, 1H), 4.87 (d, *J* = 7.0 Hz, 1H), 3.85 (s, 3 H), 3.33 (dd, *J* = 13.9, 5.5 Hz, 1H), 3.21 (dd, *J* = 13.9, 6.5 Hz, 1H), 1.42 (s, 9 H). ^{13}C NMR (151 MHz, $CDCl_3$) δ 198.27, 170.09, 155.20, 151.46, 142.66, 141.33, 135.99, 133.74, 129.66, 128.71, 127.57, 127.25, 123.37, 121.59, 111.43, 80.19, 55.96, 54.50, 38.26, 28.40, 27.67.

General method for synthesis of mono-carbonyl curcumin amino acid conjugates H1-H6

Compounds **3a**-**3f** (2 mmol) were allowed to react with 15 mL of 2 mol/L hydrochloric acid methanol solution at 0 °C for 2–3 h, and TLC was used to monitor the reaction progress. After reaction completion, the product was filtered, dried, and purified by recrystallization using ethanol and petroleum ether. This process yielded target compounds **H1-H6** with 72–78% yields. (**H1**) Yield: 77%. ESI-MS *m*/*z*: 439.45 (M-H)$^-$. (**H2**) Yield: 73%. ESI-MS *m*/*z*: 467.51 (M-H)$^-$. (**H3**) Yield: 72%. ESI-MS *m*/*z*: 523.61 (M-H)$^-$. (**H4**) Yield: 72%. ESI-MS *m*/*z*: 551.67 (M-H)$^-$. (**H5**) Yield: 78%. ESI-MS *m*/*z*: 587.73 (M-H)$^-$. (**H6**) Yield: 75%. ESI-MS *m*/*z*: 619.70 (M-H)$^-$.

Inhibition effect on cell proliferation in HepG2 cells

The cell proliferation activity of curcumin derivatives **H1-H6** towards HepG2 cells was evaluated via MTT assay and clone formation assay. As shown in Fig. 2A, the cell monolayer was incubated with six conjugates of mono-carbonyl curcumin with amino acids **H1-H6** at the concentration of 10 μM for 48 h. Curcumin and sorafenib were used as positive controls. It was obvious that all of these conjugates except **H6** exhibited more potent toxicity in HepG2 cells when compared with the blank control (only cells sap added group) and curcumin group. Remarkably, derivative **H1** was the most active compound and showed equivalent activity to the positive drug sorafenib, which was chosen for further studies. As shown in Fig. 2B, the cells were treated with **H1** at different concentrations (0.5, 1, 2, 4, 8, 16, 32, 64 μM) for 48 h. The IC_{50} values of **H1** and curcumin were 8.66 and 36.19 μM, respectively and the anti-proliferation activity of **H1** was about 4.18 times higher than that of curcumin. As shown in Fig. 2C, the clone formation assay also displayed that **H1** (4 μM) inhibited the clone formation ability of HepG2 cells for 48 h. The results of MTT and clone formation assay indicated that **H1** exhibited promising anti-proliferation activity in HepG2 cells.

Inhibition migration and apoptosis-inducing effects

To verify whether derivative **H1** has the anti-migration effect, a wound healing test and transwell migration assay were applied to the test. The results of the wound healing assay in Fig. 3A indicated that after treating HepG2 cells with 4 μM **H1** for 24 h and 48 h, the relative migration distance of cells was markedly reduced in a time-dependent manner compared to the control cells and curcumin. The results of the transwell migration assay in Fig. 3B showed that the number of traveling through the filter was significantly decreased with **H1** (4 μM) for

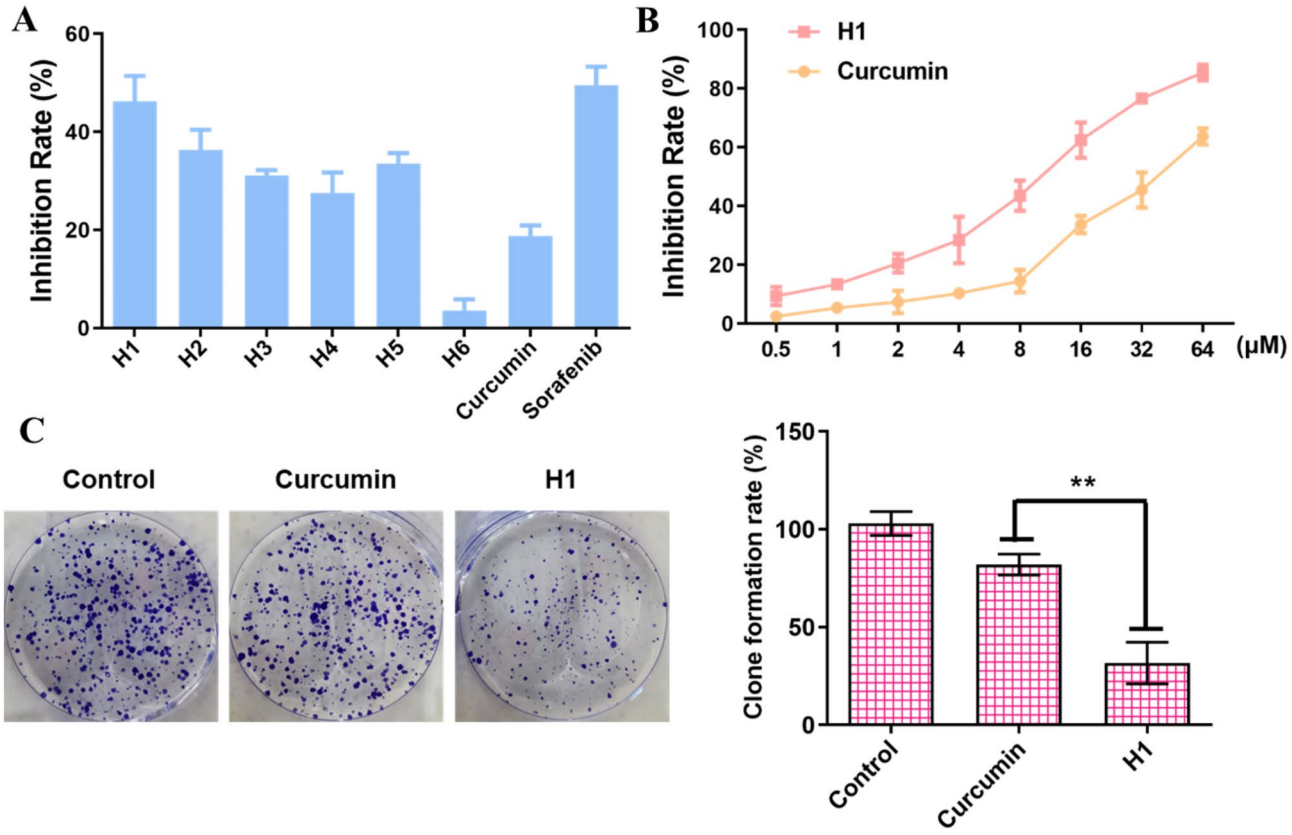

Fig. 2. Anti-proliferation assay to HepG2 cells in vitro. (A) Curcumin derivatives **H1-H6** at the concentration of 10 μM for 48 h compared with curcumin and sorafenib. (B) **H1** and curcumin at different concentrations (0.5, 1, 2, 4, 8, 16, 32, 64 μM) for 48 h. (C) Clone formation assay to HepG2 cells treatment with **H1** (4 μM) for 2 weeks. Data was represented by the mean ± SD of the three independent experiments. $^{**}P < 0.01$, compared with the curcumin group.

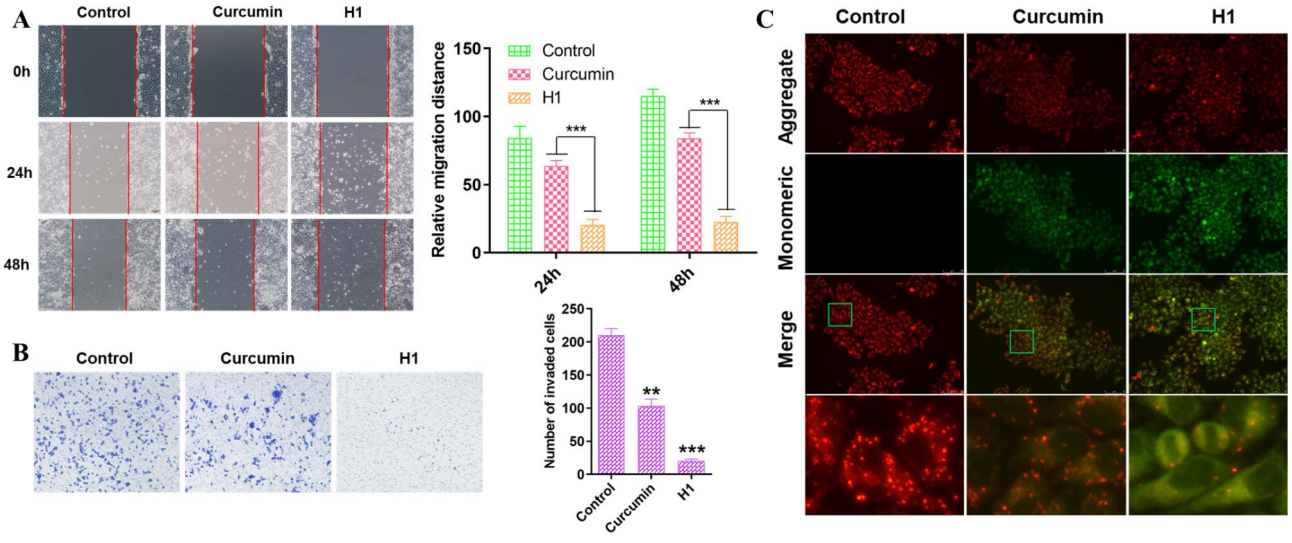

Fig. 3. Wound healing assay (A) and transwell migration assay (B) to HepG2 cells treatment with DMEM medium containing the indicated concentrations (4 μM) of **H1** for 24 h and 48 h. (C) Analysis of apoptotic HepG2 cells by JC-1 staining assay. The cell was treated with **H1** (4 μM) for 48 h, and then stained with JC-1 for 20 min at 37 ℃. The representative images were shown of the corresponding fluorescent channel (40×magnification). Data was represented by the mean ± SD of the three independent experiments. $^{***}P < 0.001$, $^{**}P < 0.01$, compared with the control group.

48 h. The results of the wound healing test and transwell migration assay together suggested that **H1** exhibited the strong potential to suppress HepG2 cell migration and hence inhibit tumor progression.

We next performed a metachromatic fluorochrome JC-1 staining assay to confirm whether compound **H1** can induce apoptosis. As shown in Fig. 3C, HepG2 cells were treated with compound **H1** (4 μM) for 48 h and then stained with JC-1 for 20 min at 37 °C. Both the loss of red fluorescence and the gain of green-emitting monomers indicated that compound **H1** induced apoptosis in the HepG2 cell via depolarizing mitochondrial transmembrane potential.

Antitumor activity in vivo

Due to the remarkable anti-proliferative, anti-migration and apoptosis induction activities of **H1** in vitro, its anticancer activity in vivo was assessed utilizing a mouse hepatic carcinoma cancer xenograft model established by the subcutaneous inoculation of HepG2 cells. When the tumor volumes reached approximately 100 mm^3, the mice were randomized into 3 groups with 6 mice in each group. Taking an injection of saline as the solvent vehicle control, curcumin (5 mg/kg) and **H1** (5 mg/kg) of 200 μL were injected into mice intraperitoneally administered every day for 27 days. The body weight (Fig. 4A) and tumor volume (Fig. 4B) of the random selection of nude mice were recorded every three days. During treatment, all the animals in different treatment groups were kept at relatively stable body weights, suggesting the low toxicity of **H1**. When the tumors were dissected and weighed after compound treatment, the inhibition rate of the average tumor volume of **H1**-treated mice was significantly better than curcumin. Then, H&E staining of rat liver cells was conducted to observe the difference in cell morphology in different groups of tumor tissues. As illustrated in Fig. 4C, the results showed that curcumin derivative **H1** destroyed the cell structure of transplanted tumor tissues, resulting in the blue-stained nucleus disappearing and the cells and tissues necrotizing. Overall, these findings indicated that curcumin derivative **H1** effectively inhibited cancer growth in vivo and represented a promising drug candidate for hepatocellular carcinoma.

Curcumin-Induced comprehensive transcriptomes profile in HepG2 cells

To explore the underlying mechanism of curcumin, we drew a comprehensive transcriptome sequencing technology and data analysis mining of HepG2 liver cancer cells in Fig. 5. We found that a total of 5793 differentially expressed genes (DEGs) were significantly up-regulated and 2295 genes down-regulated in the curcumin intervention group compared with the control group. Gene Ontology (GO) and Kyoto Encyclopedia of Genes and Genomes (KEGG) enrichment analysis were applied to explore the role of DEGs under curcumin treatment.

The results showed that in the GO database, the DEGs after curcumin administration were mainly enriched in the regulation of transcription of DNA or RNA, transcription factor activity, DNA replication, intracellular signal transduction, response to extracellular stimuli and regulation of apoptosis, suggesting that curcumin can regulate intracellular signal transduction and the transcription factor activity to affect cell cycle and cell proliferation. In the KEGG database, the DEGs after drug administration were mainly focused on the PI3K/AKT signaling pathway, FOXO signaling pathway, transcriptional misregulation in cancers, Rap1 signaling pathway, p53 signaling pathway, MAPK signaling pathway, cAMP signaling pathway. It is suggested that curcumin may regulate multiple signaling pathways and affect cell cycle and proliferation after administration.

The results of GO and KEGG both indicated that the AKT signaling pathway and FOXO pathway might be involved in the regulation mechanism of curcumin against hepatocellular carcinoma HepG2, providing new ideas for clinical treatment and new drug development.

Pathological staging and survival analysis

The clinical importance of these genes named AKT and FOXO1 was analyzed using survival analysis and pathological staging based on gene expression levels in Fig. 6. The expressions of FOXO1 in 369 tumor tissues were significantly lower than those in 160 normal tissues in LIHC (Liver hepatocellular carcinoma), while the expression of AKT was no significant difference ($P \geq 0.05$). The results of pathological staging revealed that the expressions of AKT and FOXO1 were negatively correlated with the pathological stage of the tumor from stage I to IV. However, the F-value was 2.58 and the corresponding P-value was 0.0536 of AKT by using one-way ANOVA analysis, indicating that there was no significant difference ($P \geq 0.05$) in the expression of AKT in different stages of LIHC, which was similar to FOXO1. The overall survival of patients with LIHC with high expression of AKT was significantly shorter than that of patients with low expressions of this gene, indicating that the prognosis of patients with low AKT expression was significantly better than that of patients with high expression. On the contrary, the overall survival of patients with high expression of FOXO1 in tumor tissues was longer than that of patients with low expression of this gene. Therefore, AKT and FOXO1 might be the potential biomarkers and therapeutic targets related to the progression of LIHC.

Molecular docking analysis

To explore the specific binding mode of curcumin and its derivatives with AKT and FOXO1 proteins, molecular docking was conducted in this study by the Glide module in Schrodinger 2017. The crystal structure of AKT (PDB ID: 3O96, resolution: 2.70 Å, R_{free}: 0.308) and FOXO1 (PDB ID: 6AEJ, resolution: 2.80 Å, R_{free}: 0.222) were downloaded from the Protein Data Bank (www.rcsb.org). The conjugates **H1**-**H6**, endogenous ligand, mono-carbonyl curcumin and curcumin were docked by standard precision (SP) glide and flexible dock according to the protocols. As shown in Table 1, the docking score of **H1**-**H6** to AKT and FOXO1 proteins were stronger than endogenous ligand, mono-carbonyl curcumin and curcumin, which was conducive to playing a pivotal role in protein inhibition and stability. Importantly, the docking score of **H1** was the highest among all of the conjugates, which was consistent with the result of the MTT assay. Conjugates **H1** was well extended into the active pocket

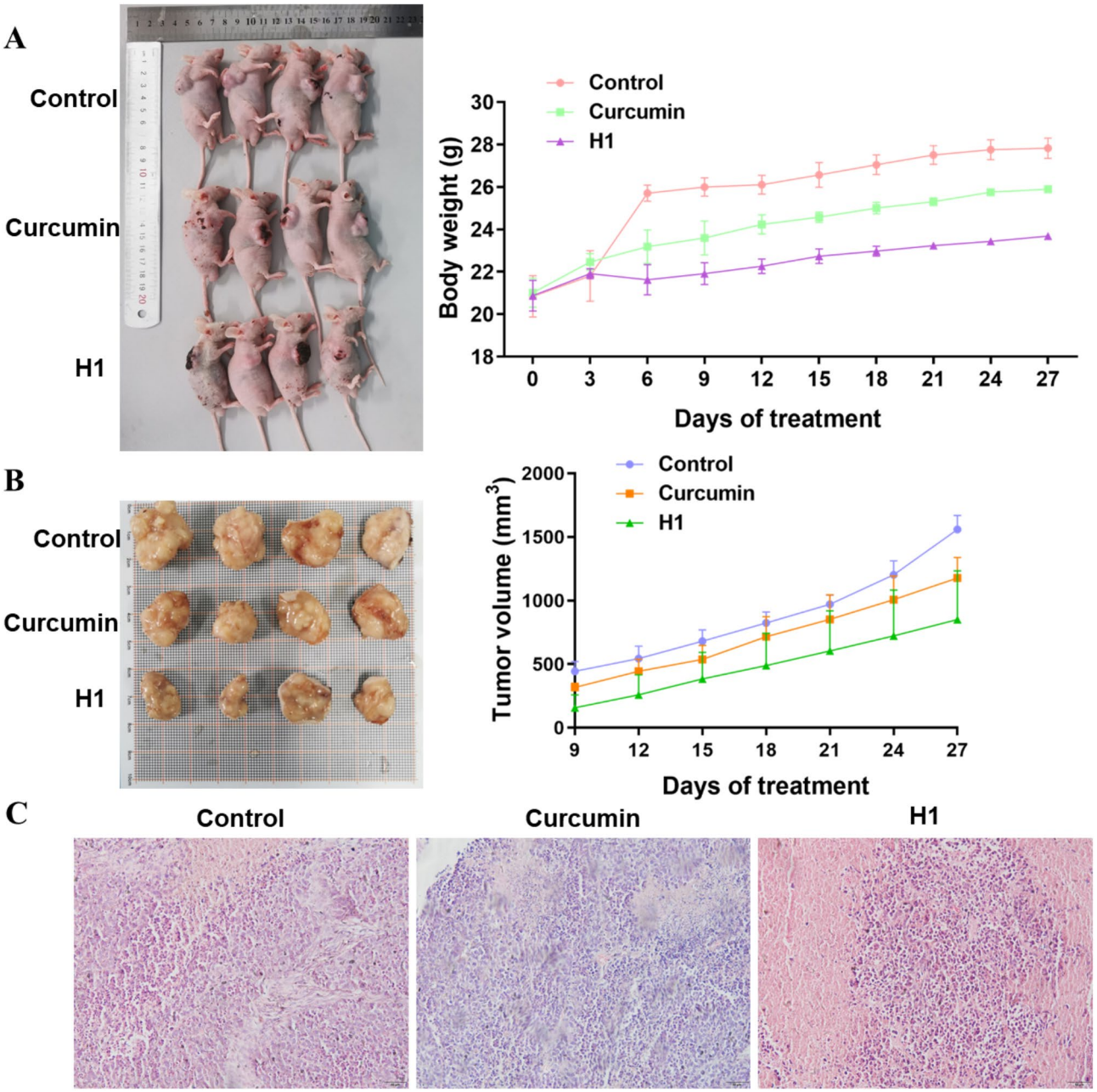

Fig. 4. Derivative **H1** inhibited HepG2 xenograft growth in vivo compared with control and curcumin. Body weight (A) and tumor volume (B) changes of mice were examined every 3 days for 27 days during treatment. Visible tumor formation and photographs of representative tumors removed from mice after treatment. (C) The xenograft tumor tissues of nude mice were observed and photographed through H&E staining (200×). Data was represented by the mean ± SD of the three independent experiments.

and bound to key residues GLU85 (2.0 Å) and SER205 (2.3 Å) of AKT through intermolecular hydrogen bonds (No shown). As shown in Fig. 7, the NH_2 group of **H1** formed H-bonds with key residues HIS232, GLU234, TYR295, ARG316 and π-π stacking with key residue HIS231. These results of molecular docking may contribute to the difference in their anti-HCC activity.

AKT/FOXO1 pathway

Previous studies revealed that curcumin and mono-carbonyl curcumin esters suppressed HCC cancer development through inhibition of the expression of AKT protein[11,37,38]. To further assess whether derivative **H1** had a similar blocking AKT function and how to regulate downstream signaling molecules, the cells were treated with different concentrations (0, 2, 4, 8 μM) of **H1** for 48 h, and cell lysates were prepared and analyzed by western blot. As shown in Fig. 8, H1 markedly suppressed the phosphorylation of AKT and up-regulated the expression of FOXO1 and P27 in a dose-dependent manner in HepG2 cells. In addition, compound **H1** (4 μM)

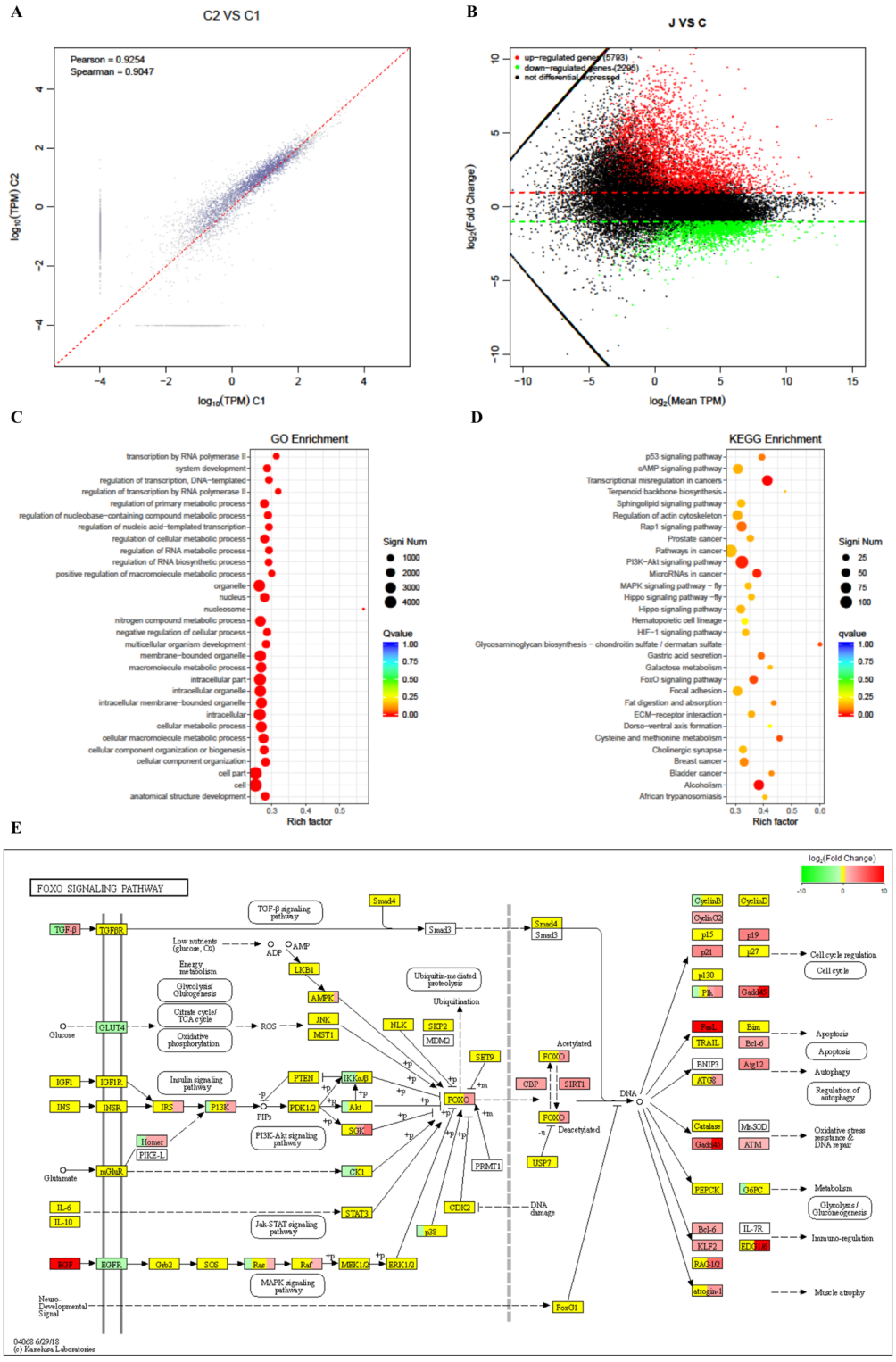

Fig. 5. Transcriptome alterations of HepG2 cells were uncovered by high-throughput sequencing. (A) Scatter plot of repeat correlation check. The horizontal and vertical axes are the $\log_{10}$(TPM) values of the two samples respectively. The more similar the samples, the closer the similarity index is to 1, and most of the points in the figure will be clustered near the diagonal. (B) MA map of comparison group expression difference. The horizontal axis is the average $\log_2$(TPM) of the two groups of samples, that is, $(\log_2(A) + \log_2(B))/2$, and the vertical axis is $\log_2$(Foldchange), that is, the $\log_2(B/A)$ value. The red, green, and black spots showed up-regulated, down-regulated, and no difference genes, respectively. (C) GO enrichment analysis. (D) KEGG enrichment analysis of the top 30 DEGs. (E) The FOXO signal pathway.

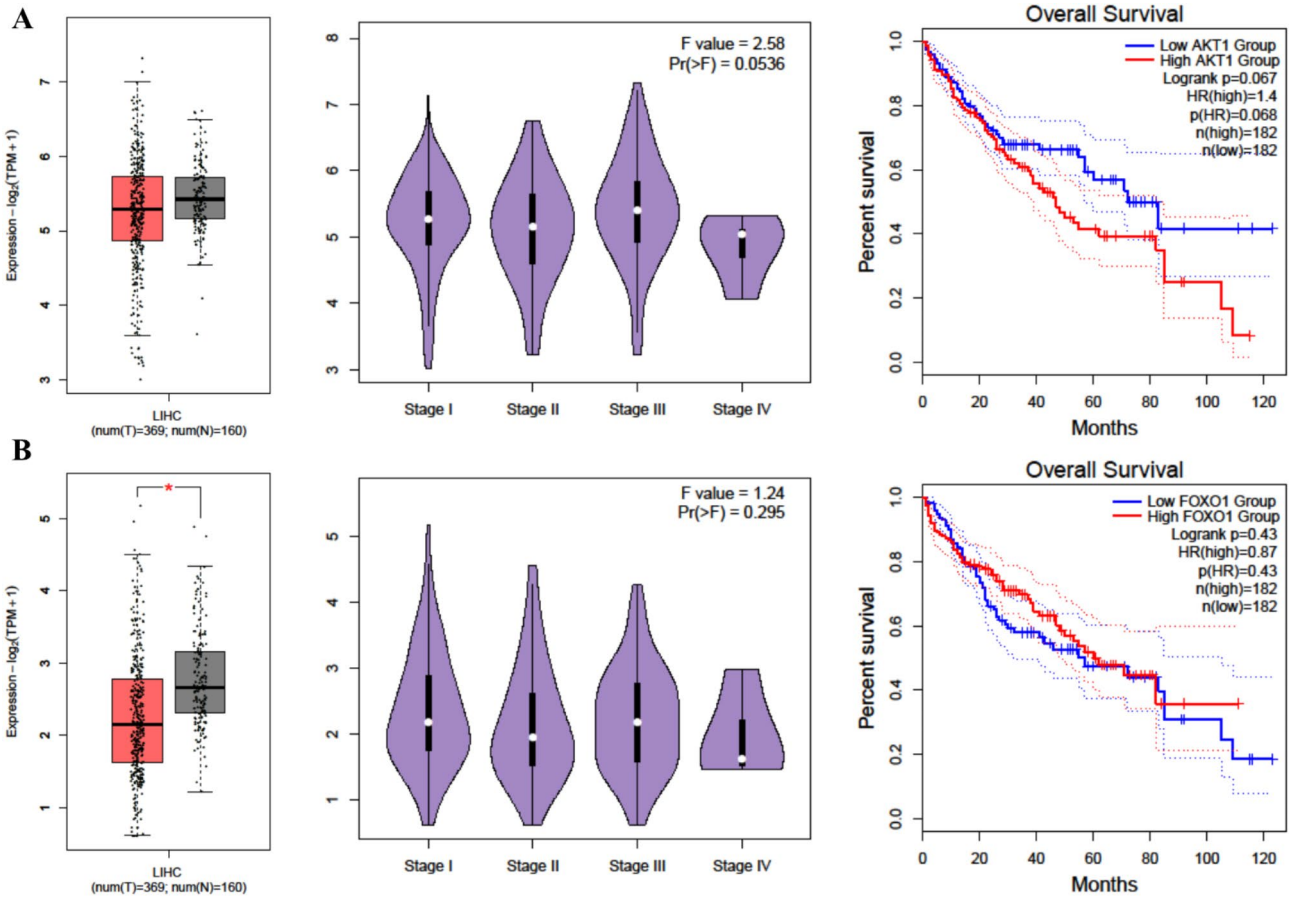

Fig. 6. The expressions of AKT (A) and FOXO1 (B) in LIHC using box plots, violin plots and survival analysis.

Conjugates	AKT protein	Conjugates	FOXO1 protein
H1	−10.486	H1	−8.771
H5	−10.198	H2	−8.293
H2	−9.947	H5	−8.291
3O96 ligand	−9.363	6AEJ ligand	−8.215
H3	−9.182	H3	−8.192
H4	−8.917	Mono-carbonyl curcumin	−8.19
Mono-carbonyl curcumin	−7.724	Curcumin	−8.089
Curcumin	−7.369	H4	−8.081
H6	−7.301	H6	−6.247

Table 1. Docking results (Kcal/mol) of SP models of **H1**-**H6** with AKT protein (3O96) and FOXO1 protein(6AEJ).

caused a significant increase in caspase-3 activation and inhibition in Bcl2 phosphorylation by western blotting with β-actin as the reference. This result indicated amino acid conjugates of mono-carbonyl curcumin **H1** could inhibit cell proliferation and induce apoptosis through the AKT/FOXO1 pathway in hepatocellular carcinoma cells.

Conclusion

To look for a lead compound with potent anti-HCC activity, we evaluated the biological activity of novel amino acid conjugates of mono-carbonyl curcumin, known as **H1**-**H6**. Remarkably, **H1** exhibited more significant activity than that of curcumin and was equivalent to the positive drug sorafenib via MTT assay in HepG2 cells. A series of pharmacological assays containing cell proliferation by clone formation assay, cell migration by wound healing and transwell assay, cell apoptosis by JC-1 staining, and the underlying mechanism were further explored by transcriptome sequence, bioinformatics analysis, molecular docking, and western blotting.

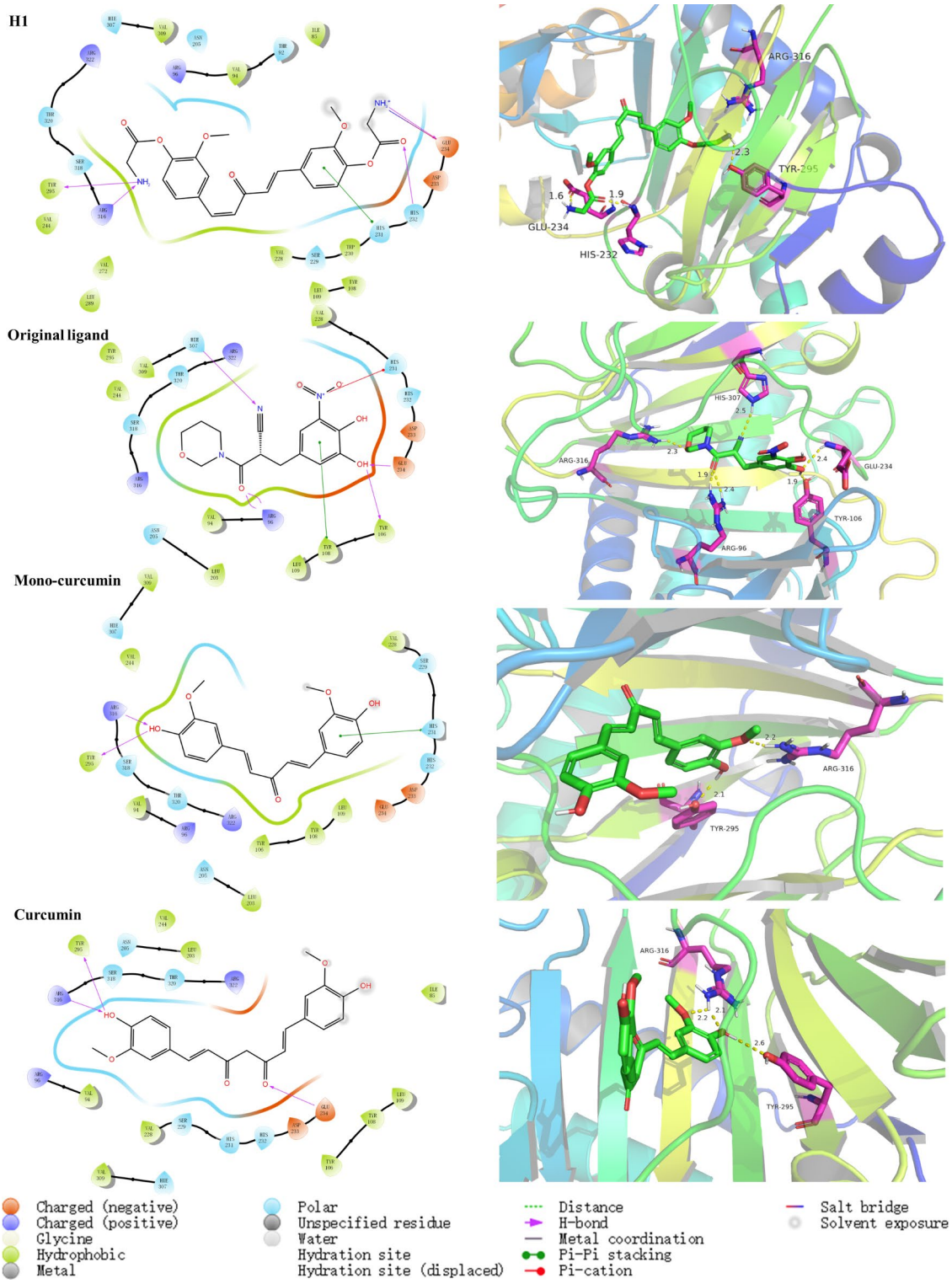

Fig. 7. The interaction pattern between derivative **H1** (A), curcumin (B), mono-carbonyl curcumin (C), endogenous ligand (D) and FOXO1 protein showed the electrostatic surface in the 2D and 3D representation from molecular docking. **H1** (green) and key residues (red) were represented in sticks and coloured by atom type.

The results showed that **H1** exerted greater potential than curcumin against liver cancer in vitro studies. The HepG2 cell xenograft model and H&E staining results also indicated that curcumin derivative **H1** had a better therapeutic effect on tumor growth. The antitumor mechanism may be related to the regulation of the AKT/FOXO1 pathway. All in all, **H1** was discovered and identified as a potent anti-hepatoma agent.

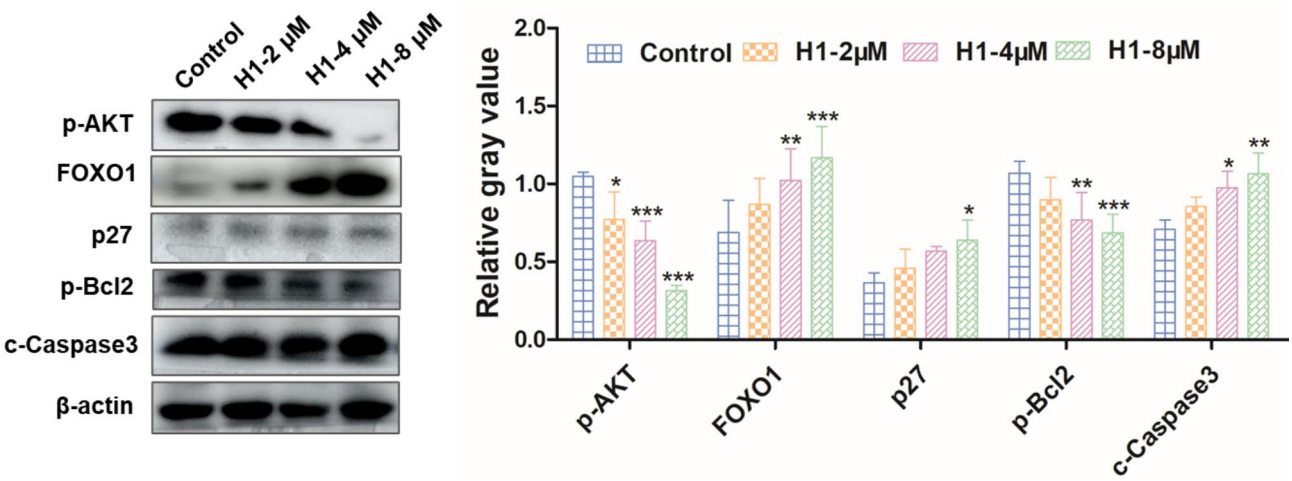

Fig. 8. Effect of derivative **H1** (0, 2, 4, 8 μM) on p-AKT, FOXO1, p27, p-Bcl2, c-Caspase3 proteins at the cell level via western blot with β-actin as the reference. Data was represented by the mean ± SD of the three independent experiments. $^{***}P < 0.001$, $^{**}P < 0.01$, $^{*}P < 0.05$, compared with the 0 μM group.

Data availability

Data will be made available on request. The data that support the findings of this study are available from the corresponding author Pan Yu upon reasonable request.

Received: 30 December 2024; Accepted: 6 March 2025
Published online: 10 March 2025

References

1. Agrawal, D. K. & Mishra, P. K. Curcumin and its analogues: potential anticancer agents. *Med. Res. Rev.* **30** (5), 818–860 (2010).
2. Noorafshan, A. & Ashkani-Esfahani, S. A review of therapeutic effects of Curcumin. *Curr. Pharm. Des.* **19** (11), 2032–2046 (2013).
3. Slika, L. & Patra, D. Traditional uses, therapeutic effects and recent advances of Curcumin: A Mini-Review. *Mini Rev. Med. Chem.* **20** (12), 1072–1082 (2020).
4. Zhao, S. et al. Recent advances of analogues of Curcumin for treatment of cancer. *Eur. J. Med. Chem.* **180**, 524–535 (2019).
5. Anand, P. et al. Bioavailability of Curcumin: problems and promises. *Mol. Pharm.* **4** (6), 807–818 (2007).
6. Ireson, C. R. et al. Metabolism of the cancer chemopreventive agent Curcumin in human and rat intestine. *Cancer Epidemiol. Biomarkers Prev.* **11** (1), 105–111 (2002).
7. Zhao, C., Liu, Z. & Liang, G. Promising Curcumin-based drug design: mono-carbonyl analogues of Curcumin (MACs). *Curr. Pharm. Des.* **19** (11), 2114–2135 (2013).
8. Pan, Z. et al. Synthesis and cytotoxic evaluation of monocarbonyl analogs of Curcumin as potential Anti-Tumor agents. *Drug Dev. Res.* **77** (1), 43–49 (2016).
9. Reddy, A. R. et al. A comprehensive review on SAR of Curcumin. *Mini Rev. Med. Chem.* **13** (12), 1769–1777 (2013).
10. Rodrigues, F. C., Anil Kumar, N. V. & Thakur, G. Developments in the anticancer activity of structurally modified Curcumin: an up-to-date review. *Eur. J. Med. Chem.* **177**, 76–104 (2019).
11. Yu, P. et al. Design, synthesis, and antitumor evaluation of novel Mono-Carbonyl Curcumin analogs in hepatocellular carcinoma cell. Pharmaceuticals (Basel), 15(8) (2022).
12. Cao, W. et al. Discovery of novel Mono-Carbonyl Curcumin derivatives as potential Anti-Hepatoma agents. *Molecules*, **28**(19). (2023).
13. Kelly, B. & Pearce, E. L. Amino assets: how amino acids support immunity. *Cell. Metab.* **32** (2), 154–175 (2020).
14. Durante, W. Amino acids in circulatory function and health. *Adv. Exp. Med. Biol.* **1265**, 39–56 (2020).
15. Lau, J. L. & Dunn, M. K. Therapeutic peptides: historical perspectives, current development trends, and future directions. *Bioorg. Med. Chem.* **26** (10), 2700–2707 (2018).
16. Fu, X. Y. et al. Three rounds of Stability-Guided optimization and systematical evaluation of oncolytic peptide LTX-315. *J. Med. Chem.* **67** (5), 3885–3908 (2024).
17. Yin, H. et al. The hybrid oncolytic peptide NTP-385 potently inhibits adherent cancer cells by targeting the nucleus. *Acta Pharmacol. Sin.* **44** (1), 201–210 (2023).
18. Yin, H. et al. Design, synthesis and anticancer evaluation of novel oncolytic peptide-chlorambucil conjugates. *Bioorg. Chem.* **138**, 106674 (2023).
19. Arifian, H. et al. Amino-Acid-Conjugated natural compounds: aims, designs and results. *Molecules*, **27**(21). (2022).
20. Manjunatha, J. R. et al. Synthesis of amino acid conjugates of Tetrahydrocurcumin and evaluation of their antibacterial and anti-mutagenic properties. *Food Chem.* **139** (1–4), 332–338 (2013).
21. Ni, J. et al. Preparation of valine-curcumin conjugate and its in vitro antibacterial and antitumor activity and in vivo biological effects on American Eels (Anguilla rostrata). *Fish. Shellfish Immunol.* **149**, 109615 (2024).
22. Kim, M. K. et al. In vitro solubility, stability and permeability of novel quercetin-amino acid conjugates. *Bioorg. Med. Chem.* **17** (3), 1164–1171 (2009).
23. Fang, L. et al. Combination of amino acid/dipeptide with nitric oxide donating oleanolic acid derivatives as PepT1 targeting antitumor prodrugs. *J. Med. Chem.* **57** (3), 1116–1120 (2014).
24. Dubey, S. K. et al. Design, synthesis and characterization of some bioactive conjugates of Curcumin with Glycine, glutamic acid, valine and demethylenated piperic acid and study of their antimicrobial and antiproliferative properties. *Eur. J. Med. Chem.* **43** (9), 1837–1846 (2008).

25. Qi, Y. K., Zheng, J. S. & Liu, L. Mirror-image protein and peptide drug discovery through mirror-image phage display. *Chem* **10** (8), 2390–2407 (2024).
26. Yu, P. et al. Synthesis and antitumor activity of C-3(R) hydroxy modified betulinic acid derivatives. *Chem. Nat. Compd.* **55** (6), 1080–1084 (2019).
27. Cao, W. et al. Autophagy up-regulated by MEK/ERK promotes the repair of DNA damage caused by aflatoxin B1. *Toxicol. Mech. Methods.* **32** (2), 87–96 (2022).
28. Cao, W. et al. Curcumin reverses hepatic epithelial mesenchymal transition induced by trichloroethylene by inhibiting IL-6R/STAT3. *Toxicol. Mech. Methods.* **31** (8), 589–599 (2021).
29. Yu, P. et al. *Design, synthesis and antitumor evaluation of novel Quinazoline analogs in hepatocellular carcinoma cell. J. Mol. Struct.*, 1268. (2022).
30. Wang, P. F. et al. Identification of novel B-Raf(V600E) inhibitors employing FBDD strategy. *Biochem. Pharmacol.* **132**, 63–76 (2017).
31. Kong, Y. et al. Discovery and structural optimization of 9-O-phenylsulfonyl-berberines as new lipid-lowering agents. *Bioorg. Chem.* **121**, 105665 (2022).
32. Sherman, B. T. et al. DAVID: a web server for functional enrichment analysis and functional annotation of gene lists (2021 update). *Nucleic Acids Res.* **50** (W1), W216–W221 (2022).
33. Tang, Z. et al. GEPIA2: an enhanced web server for large-scale expression profiling and interactive analysis. *Nucleic Acids Res.* **47** (W1), W556–W560 (2019).
34. Yu, P. et al. Identification of dihydroorotate dehydrogenase as a protein target of ginkgolic acid by molecular Docking and dynamics. *J. Mol. Struct.*, 1220. (2020).
35. Wu, W. I. et al. Crystal structure of human AKT1 with an allosteric inhibitor reveals a new mode of kinase Inhibition. *PLoS One.* **5** (9), e12913 (2010).
36. Yu, P., Cao, W. & Wang, Y. Dynamics simulation and in vitro studies of betulinic acid derivative with liver X receptor. *J. Biomol. Struct. Dyn.*, pp. 1–10. (2023).
37. Mou, S. et al. Curcumin inhibits cell proliferation and promotes apoptosis of laryngeal cancer cells through Bcl-2 and PI3K/Akt, and by upregulating miR-15a. *Oncol. Lett.* **14** (4), 4937–4942 (2017).
38. Rana, C. et al. Downregulation of PI3-K/Akt/PTEN pathway and activation of mitochondrial intrinsic apoptosis by diclofenac and Curcumin in colon cancer. *Mol. Cell. Biochem.* **402** (1–2), 225–241 (2015).

Acknowledgements

This work was supported by the Scientific Research Foundation for High-level Talents of Anhui University of Science and Technology (NO. 2022yjrc69), Joint Research Center of Occupational Medicine and Health, Institute of Grand Health, Hefei Comprehensive National Science Center (Anhui University of Science and Technology) (NO. OMH-2023-14), Medical Special Cultivation Project of Anhui University of Science and Technology (NO. YZ2023H1B005), Natural Science Research Project of Anhui Educational Committee (No. KJ2021A0436), Anhui Provincial Natural Science Foundation (NO. 2108085QH381).

Author contributions

W.C. and P.Y. conceived and designed the experiments. W.C., Y.C., S.F., N.Y. performed the experiments. W.C. and P.Y. analyzed the data and wrote the paper. All authors reviewed and approved the manuscript .

Declarations

Competing interests

The authors declare no competing interests.

Additional information

Supplementary Information The online version contains supplementary material available at https://doi.org/10.1038/s41598-025-93451-1.

Correspondence and requests for materials should be addressed to P.Y.